

Anomalous orbital structure in two-dimensional titanium dichalcogenides

Banabir Pal,^{1,*} Yanwei Cao,^{1,2,†} Xiaoran Liu,¹ Fangdi Wen,¹ M. Kareev,¹ A. T. N'Diaye,³ P. Shafer,³ E. Arenholz,³ and J. Chakhalian¹

¹*Department of Physics and Astronomy, Rutgers University, Piscataway, New Jersey 08854, USA*

²*Ningbo Institute of Materials Technology and Engineering,
Chinese Academy of Sciences, Ningbo, Zhejiang 315201, China*

³*Advanced Light Source, Lawrence Berkley National Laboratory, Berkeley, California 94720, USA*

(Dated: April 24, 2018)

Generally, lattice distortions play a key role in determining the ground states of materials. Although it is well known that trigonal distortions are generic to most two dimensional transition metal dichalcogenides, the impact of this structural distortion on the electronic structure has not been understood conclusively. Here, by using a combination of polarization dependent X-ray absorption spectroscopy (XAS), X-ray photoelectron spectroscopy (XPS) and atomic multiplet cluster calculations, we have investigated the electronic structure of titanium dichalcogenides TiX_2 ($\text{X}=\text{S}, \text{Se}, \text{Te}$), where the magnitude of the trigonal distortion increase monotonically from S to Se and Te. Our results reveal the presence of an anomalous and large crystal field splitting. This unusual kind of crystal field splitting is likely responsible for the unconventional electronic structure of TiX_2 compounds. Our results also indicate the drawback of the distorted crystal field picture in explaining the observed electronic ground state of these materials and emphasize the key importance of metal-ligand hybridization and electronic correlation in defining the electronic structures near Fermi energy.

The realization of numerous exotic electronic phases of graphene^{1–3} and the relentless tendency to miniaturization of silicon-based electronics⁴ have ignited exhaustive research in a wide range of two dimensional (2D) layered materials. As a result, 2D transition metal dichalcogenides have emerged as the promising platform with intriguing electronic ground states and high potential for applicability in the field of microelectronics^{5,6}, nanophotonics^{7,8}, optoelectronics^{9,10} and photovoltaics^{11–13} to name a few. A generic feature of this dichalcogenide family is the presence of structural distortions which play a critical role in defining the electronic ground state of these systems. Specifically, lattice deformations in chalcogenides invariably alter the interatomic interaction strength and thereby produces various novel electronic phases including charge density wave in VSe_2 ^{14,15}, NbSe_2 ¹⁶ and TaSe_2 ^{17,18}, superconductivity in $\text{FeSe}_{1-x}\text{Te}_x$ ¹⁹, insulating ground states in ReSe_2 ²⁰, Weyl semi-metallic phase in MoTe_2 ²¹ and more. Naturally, a proper understanding of the lattice distortions and their impact on the electronic structure are essential for deterministic control of the rich physical properties of these 2D systems.

Recently, titanium dichalcogenides TiX_2 (here $\text{X} = \text{S}, \text{Se}$ and Te) have attracted significant attention of the community as potential candidates for energy storage applications^{22–25} due to the easily achievable lithium intercalation. While the usual crystallographic form of TiX_2 is the layered CdI_2 type²⁶, these systems also possess a distinct trigonal distortion from an ideal octahedral crystal environment^{26,27}. Previously, de-

tailed structural investigation established that the magnitude of the distortion varies monotonically from nearly octahedral in TiS_2 ²⁶ to highly distorted in TiTe_2 ²⁷. In addition, large body of work on transition metal compounds suggest that these generic trigonal distortions may have strong influence in modifying the energy level and electronic structure of the chalcogenides. The problem is vividly illustrated by the case of TiSe_2 which undergoes the transition into a chiral charge density wave (CDW) state^{28,29} and further into a conventional CDW resulting in dramatic renormalization of electronic and structural properties. The fundamental challenge here is to separate the many-body effects associated with excitonic condensate^{30–32} from the Jahn-Teller like instability from the strong-electron phonon coupling^{33,34}. In addition, recent extensive theoretical work based on LDA+U³⁵ along with the detailed ARPES³⁶ study hinted on the importance of lattice distortions coupled with strong electron-electron correlations to explain the ground state properties of TiSe_2 . Based on those findings and given the obvious importance of these the whole TiX_2 family, there have been several experimental and theoretical investigations to understand the impact of trigonal distortion on the electronic structure in these systems^{37–39}. However, in absence of systematic spectroscopic investigations corroborated with theoretical calculations the consequence of the trigonal distortion on the electronic structure of the TiX_2 systems has not convincingly been reported thus far. Here, we have addressed this issue by investigating the whole family of TiX_2 single crystals by means of

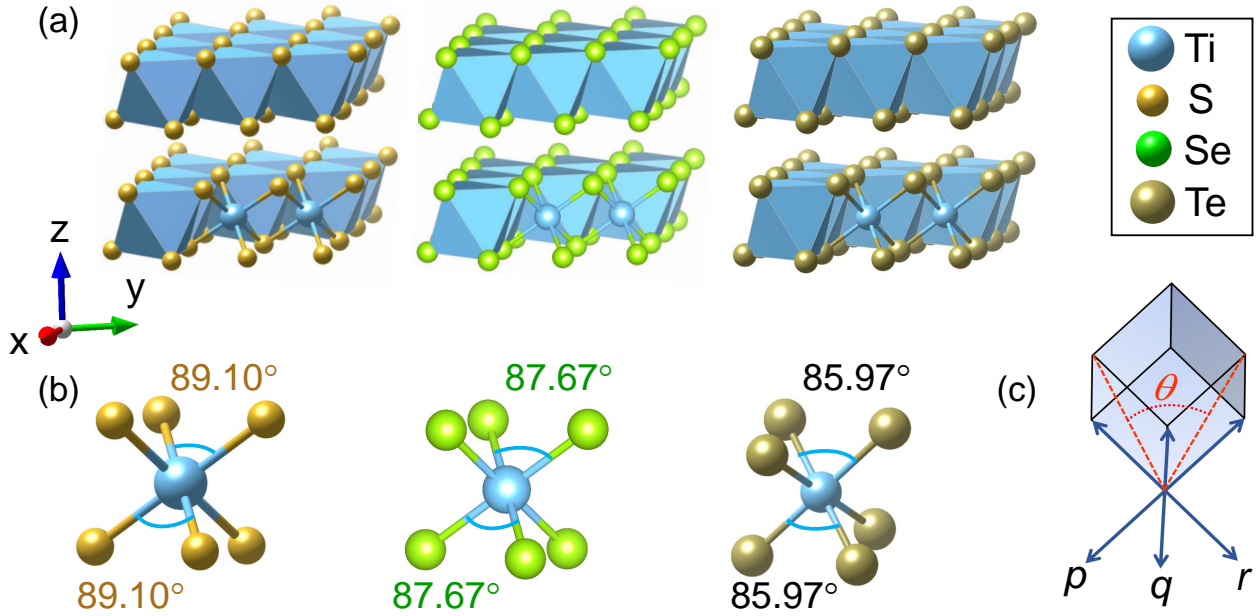


FIG. 1. (a) Schematic crystal structure of the TiS_2 , TiSe_2 , and TiTe_2 compounds showing nearly octahedral environment of each TiX_2 unit. (b) Distortion of the ideal octahedral environment across the chalcogenide series. It is to be noted that the distortion does not change the bond length but alters the bond angle. (c) Schematic representation of the trigonal distortions.

polarization dependent X-ray absorption spectroscopy in conjunction with the multiplet cluster calculations. Our results unambiguously demonstrate the failure of the standard ionic configuration and distorted crystal field picture in predicting electronic ground states and thereby reveal the key importance of metal-ligand hybridization between titanium and chalcogen ions and electronic correlations in defining their electronic properties.

As shown in Fig. 1(a), all members of the TiX_2 family crystallize into trigonal CdI_2 type layered structure with space group P_{3m1} ²⁶. The crystal structure consists of repeated tri-layers (Fig. 1(a)) along z direction; each tri-layer contains a titanium layer sandwiched between two layers of chalcogenides. Although the interactions between titanium and chalcogenides are strong within a tri-layer, the chalcogen bonding between two tri-layers is weak and dominated by the van der Waals type interaction. Each tri-layer further experiences an elongated trigonal distortion where all six Ti-X bond length remains constant but X-Ti-X bond angle deviates from an ideal 90° in such a manner that the crystallographic lattice parameter along z direction increases in length. As illustrated in Fig. 1(b) the strength of elongated trigonal distortion increases monotonically from TiS_2 to TiTe_2 with three different X-Ti-X bond angles. The magnitude of such elongated trigonal distortion can be estimated from c/a ratio where c and a represent the corresponding unit cell parameter along z and x

direction, respectively; For an ideal octahedral environment, the c/a ratio is close to 1.633 whereas the c/a ratio for TiS_2 , TiSe_2 and TiTe_2 are found to be 1.726, 1.732 and 1.808, respectively. This type of structural distortion can also be alternatively explained in terms of the distortion angle Θ between the diagonals of the pq , qr , rp plane as schematically shown in Fig 1(c). For a regular octahedron $\Theta = 60^\circ$ and becomes lesser and greater than 60° for elongated and compressive trigonal distortions, respectively.

Chemical quality, and the absence of chalcogen vacancies critical for most dichalcogenides are verified by X-ray photo electron spectroscopy (XPS) measurements carried out on freshly cleaved TiX_2 single crystals to rule out the presence of any anion vacancies. The basic process associated with the XPS technique is shown schematically in Fig. 2(a). Generally, the chemical shift associated with each core level provides important information about the charge state of the different elements of the system under investigation. Figure 2(b) displays typical Ti $2p$ core level spectra for three different TiX_2 systems (Core level XPS spectra of Chalcogenides are shown in supporting information). Each Ti $2p$ core-level spectrum shown in Fig.2(b) is composed of two intense spin-orbit split doublet (marked as A and B) with a spin-orbit splitting strength close to 5.8 eV. Feature A appearing at a binding energy range between 454 eV to 459 eV represents Ti $2p_{3/2}$ like states whereas feature B arises mainly from Ti $2p_{1/2}$ like

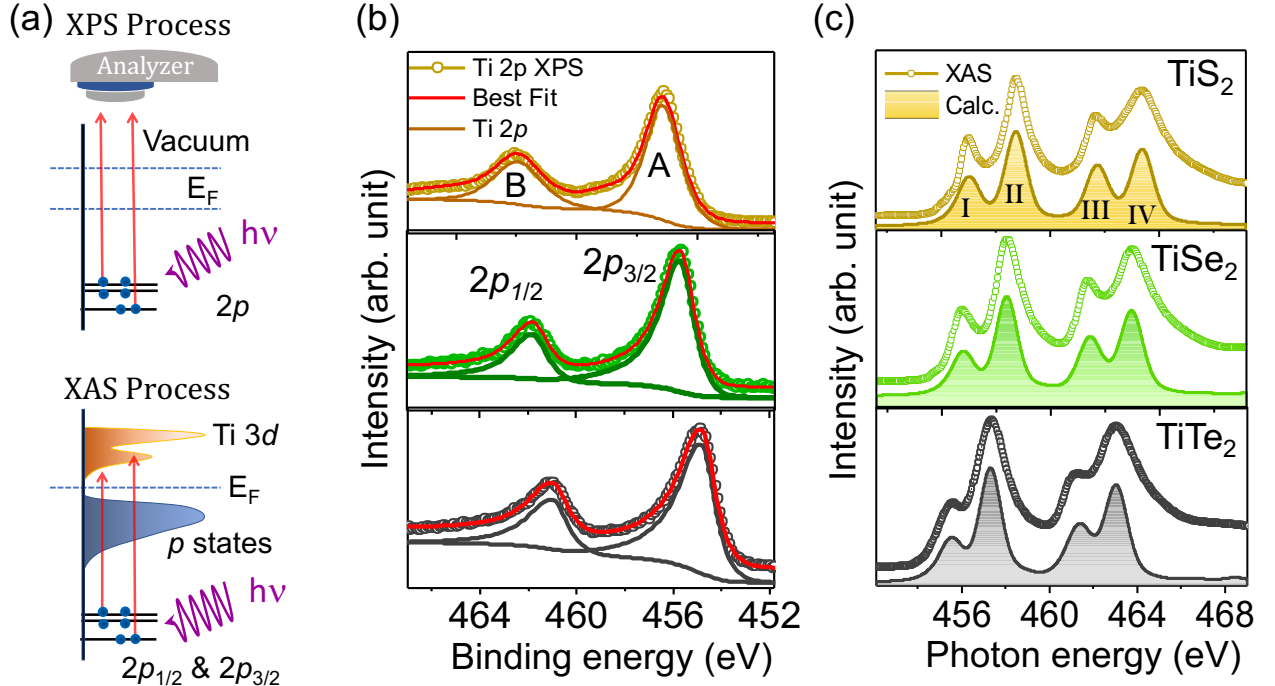


FIG. 2. (a) Schematic representations of the X-ray photoelectron (top) and X-ray absorption (bottom) spectroscopy process. (b) X-ray photoelectron spectra of Ti 2p core level. Each spectrum was decomposed with Lorentzian function convoluted with Gaussian functions. (c) Experimental XAS spectra (open circle) of three different TiX₂ systems were compared with atomic multiplet calculations (shaded area).

states. Interestingly, a systematic shift was found in moving from higher to lower binding energy in Ti 2p core level spectra from TiS₂ to TiTe₂, respectively. These shifts in the binding energy were previously attributed to the reduction in ionic contribution in Ti-X chemical bond formations⁴⁰. In this work, each spectrum was decomposed using a Gaussian-Lorentz line profile and a Shirley type background function and can be accounted within a single Gaussian-Lorentz line profile. The absence of the multiple peak structure in Ti 2p core level spectra clearly implies the presence single valence Ti, and rules out any signature of anion vacancies in our TiX₂ samples.

To investigate the evolutions in electronic structure across the TiX₂ series, XAS measurements were carried out on Ti L_{2,3} edge at beamline 4.0.2 of the Advanced Light Source, at Lawrence Berkeley National Laboratory. In a typical Ti L_{3,2} XAS process (see bottom of Fig. 2(a)), electrons are excited from Ti 2p core level (from 2p_{3/2} and 2p_{1/2}) to the Ti 3d conduction band; each L_{3,2} XAS spectrum splits into two edges (L₂ and L₃) due to the spin-orbit coupling of Ti 2p states.

Experimentally obtained Ti L_{2,3} XAS spectra for three different TiX₂ systems are shown in Fig. 2(c) as open circles. As seen both L₃ and L₂ peaks of each spectrum exhibit a

double hump feature arising primarily from nearly octahedral crystal field effects which splits the fivefold degenerate 3d orbitals of Ti into doubly degenerate e_g and triply degenerate t_{2g} orbitals. For a quantitative understanding, theoretical atomic multiplet cluster calculations were performed within a TiX₆ cluster with O_h point group symmetry and Ti⁴⁺ ionic configuration.⁴³ The obtained calculated spectra are shown as shaded line in Fig 2(c) confirm that only one types of charge state Ti⁴⁺ is present in our samples. In good agreement with the XPS spectra, we observed a gradual shift in the XAS spectra from TiS₂ to TiTe₂. This monotonic spectral shift suggests a systematic decrease in ($U_{dd} - U_{pd}$) from TiS₂ to TiTe₂ where U_{dd} symbolizes the onsite coulomb interaction strength and U_{pd} defines the core hole interaction potential. This result indicates that in case of Te, the strongest inter-atomic $p - d$ interaction strength arises from the markedly increased metal-ligand hybridization. The summary of the relative energy position of the occupied 2p states and unoccupied 3d states of titanium obtained from XPS and XAS measurements is given schematically in Fig. 3.

Despite high XAS sensitivity to charge state and local symmetry it is still very challenging to capture the effect of trigonal distortions from non-polarized XAS measurement.

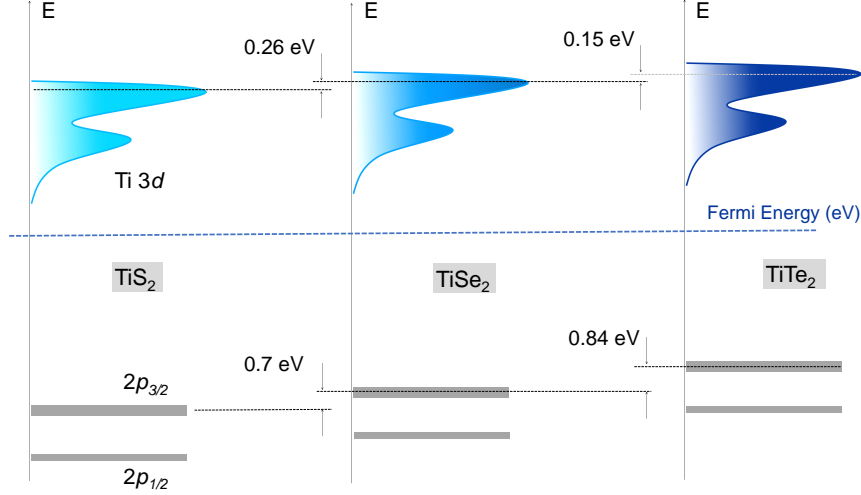


FIG. 3. (a) Band alignment of 2p and 3d states in TiS_2 , TiSe_2 and TiTe_2 as obtained from X-ray photoelectron and X-ray absorption spectroscopy.

To further explore the impact of trigonal distortion, detailed polarization dependent XAS measurements were carried out. The polarization dependent XAS process can probe local orbital character depending on their relative orientation of orbitals with respect to crystallographic axes; for example it can be sensitive to the sub-band splitting of t_{2g} states which may emerge from local lattice distortions. The polarization dependent results (in-plane vs. out-of-plane) are schematically shown in Fig. 4(a). Since our samples are aligned along their natural [111] direction, it is expected that out-of-plane polarization will be sensitive to the orbitals oriented along [111] direction whereas the in-plane polarization will probe those states which are oriented perpendicular to the [111] directions. Both out-of-plane (H) and in-plane (V) polarization dependent spectra are shown in Fig. 4(b). As immediately seen, a clear difference between the in- and out-of-plane XAS spectra is present which in turn implies the presence of distinct d -orbital anisotropy. The corresponding XLD signal or the difference between the in- and out-of-plane XAS spectrum is shown as the shaded area in Fig. 4(b) for all three samples.

To make a connection between the XLD results and orbital occupation we discuss electronic structure of the TiX_2 compounds. In the purely ionic limit, the electronic structure of these systems comprises of fully occupied p states of chalcogen atom forming valence bands and unoccupied conduction bands with the predominant Ti $3d$ character. Due to the effect of octahedral crystal field, five-fold degenerate $3d$ orbitals of Ti split into a doubly

degenerate higher energy e_g and a triply degenerate lower energy t_{2g} states⁴¹. In addition, as shown schematically in Fig. 4(c) due to elongated trigonal distortion⁴² t_{2g} states further split into a higher energy singlet a_{1g} and lower energy doublet e_g^π states. The wave function of a_{1g} and e_g^π states is a linear combination of d_{xy} , d_{yz} and d_{xz} orbitals and can be expressed as $|a_{1g}\rangle = \frac{1}{\sqrt{3}}(|xy\rangle + |yz\rangle + |xz\rangle)$ and $|e_g^\pi\rangle = \pm \frac{1}{\sqrt{3}}(|xy\rangle + e^{\mp 2i\pi/3}|yz\rangle + e^{\pm 2i\pi/3}|xz\rangle)$ ⁴⁴. The description of the mixed a_{1g} and e_g^π states becomes simplified when one assumes z axis along the [111] direction as shown in Fig. 1(a). The wave function of the a_{1g} state has a similar shape along [111] direction as the d_{z^2} orbital along [001]; e_g^π states are perpendicular to the [111] directions and oriented in xy plane (see the shape of the a_{1g} and e_g^π orbital Fig 4.(a))

Based on this picture, one would naively expect that in-plane polarization will largely probe e_g^π states which are at lower energy compared to the higher energy a_{1g} state that are more sensitive to out-of-plane polarization. Contrary to this expectation, the experimental spectra for all three systems are in complete variation with the conventional picture. More specifically, in the case of t_{2g} states labeled by feature I and III in Fig 2(c), the out-of-plane polarization (shown by solid line in Fig. 4(b)) exhibits a lower energy peak position compared to the in-plane polarization (shown by dotted line). This implies the stabilization of a_{1g} as the lowest occupied orbital contrary to the expected e_g^π state. This is completely opposite to what one would infer from the standard crystals field splitting arguments. The crystal field inversion picture is schematically shown in Fig. 4(d) (Quantitative Sub-band

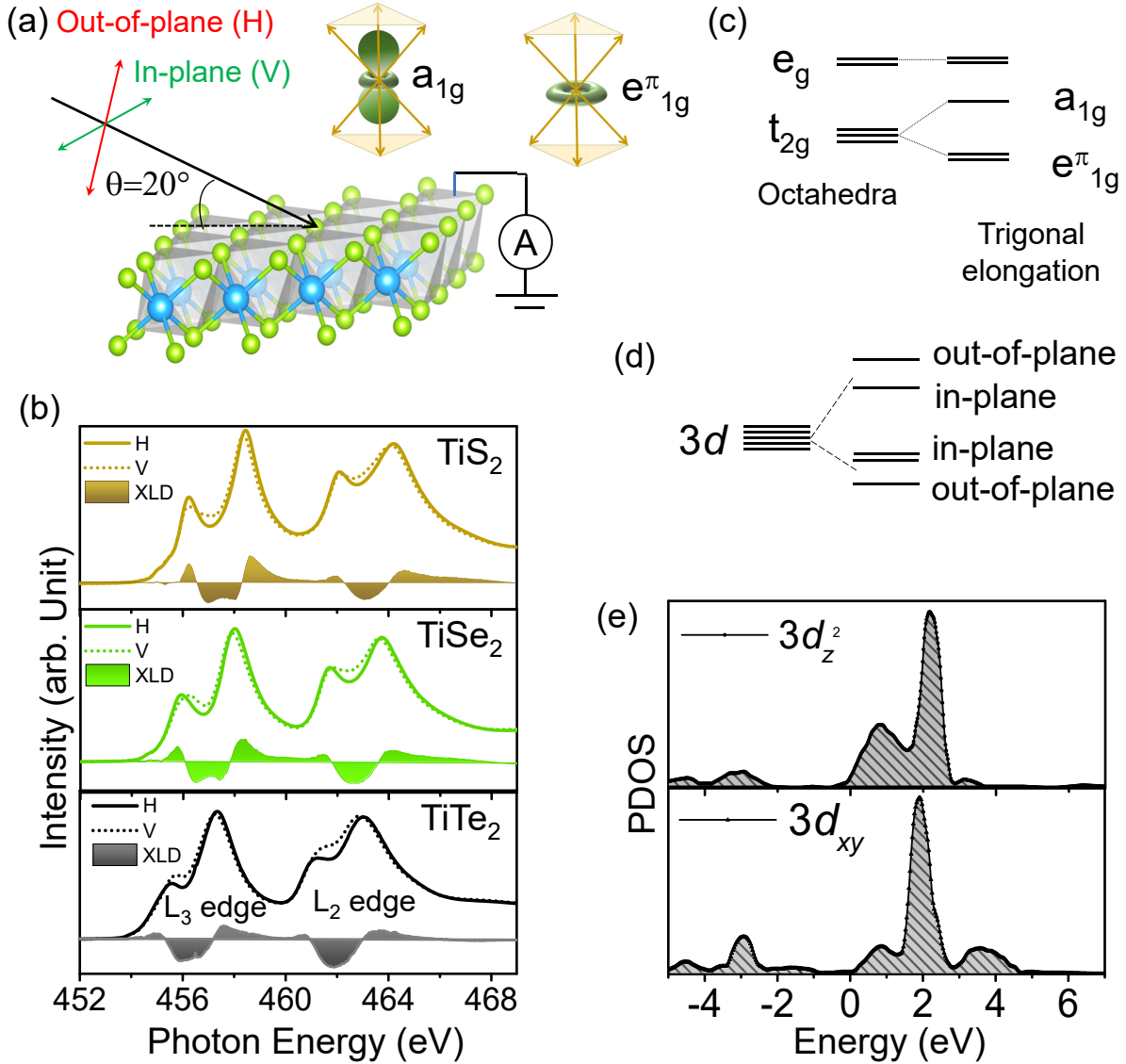


FIG. 4. (a) Experimental setup of the in-plane and out-of-plane polarization dependent XAS measurements. (b) Ti $L_{3,2}$ edge XAS/XLD spectra of three different TiX_2 compounds at room temperature. (c) Conventional theoretical model of an elongated trigonal distortion with t_{2g} sub-band splitting. (d) Experimentally observed Ti $3d$ sub-band splitting in TiX_2 . (e) PDOS of $3d_{z^2}$ and $3d_{xy}/3d_{x^2-y^2}$ obtained from previous theoretical calculations⁴⁵ on TiS_2 system where x, y, z represent global co-ordinates axis as shown schematically in Fig. 1(a)

splitting of each TiX_2 compound has been shown schematically in supporting information). These findings clearly suggest that purely ionic picture which is normally very efficient in capturing the excitation spectra of Ti^{4+} derived states in oxide systems is inadequate in explaining the origin of XLD signal in dichalcogenides. Several factors might be responsible for such discrepancy in the description of the XAS spectra. Because of the markedly enlarged p -orbitals in S, Se and especially Te, unlike oxides, covalency may

play a dominant role in transition metal dichalcogenides. The synergetic effect of high metal-ligand hybridization and significant ligand field can strongly affect the local electronic description of these systems.

Adding more to the surprising finding, the crystal field splitting gap ($10 Dq$) between t_{2g} and e_g is found to be strongly dependent on the direction of polarization of the incident light. In particular, out-of-plane polarization (solid line in Fig. 4(b)) shows a higher crystal field gap compared

to in-plane polarizations (dotted line in Fig. 4(b)). This is unexpected since for the trigonal distortion, the e_g states should not experience any sub-band splitting. However, the energy position of the e_g state is found to depend strongly on the types of polarization. All these discrepancies clearly establish that conventional crystal field picture fails to explain the observed features in these system contrary to the Ti^{4+} based oxide materials.

To resolve this inconsistency, the XAS spectra were compared with calculated projected partial density of states (PDOS) of $3d_{z^2}$ and $3d_{xy}$ states of TiS_2 ^{40,45} as shown in Fig. 4(e). Interestingly, the calculated PDOS of $3d_{z^2}$ of titanium exhibit a double hump structure analogous to the experiments when the systems were probed with out-of-plane polarization and PDOS of the $3d_{xy}/3d_{x^2-y^2}$ states (these two states are degenerate) also shows a double hump feature similar to in-plane polarization. Moreover, the energy gap between the doublet features is greater in the case of $3d_{z^2}$ PDOS as compared to $3d_{xy}$, and $3d_{x^2-y^2}$ PDOS which is remarkably similar to the experimentally observed trend. The calculated PDOS is qualitatively consistent with experimental observations and explains the appearance of the all features and their energy position as observed from experiments. The key feature of the theoretical calculation is the inclusion of strong metal-chalcogen hybridization which is responsible for the observed crystal field inversion and allows to capture the details of electronic structure within the band-like description. This result implies that indeed covalency and metal-ligand hybridization are critical for the electronic properties of the TiX_2 family of materials.

In conclusion, detailed polarization dependent XAS measurements were carried out to understand the effect of trigonal lattice distortion on the electronic structure of the TiX_2 family. All systems were characterized to rule out the presence of anion vacancies in these compounds. XLD spectra demonstrate the failure of conventional crystal field arguments in explaining the observed experimental features implying the crucial importance of covalency/metal-ligand hybridization in defining the electronic structure. Orbital projected DOS successfully reproduced the spectral features observed in our experiments. The excellent agreement between theory and the XAS spectra suggests the importance of band-like description in order to explain the electronic

structure of transition metal dichalcogenides.

Experimental Section:

XPS measurements: Ti 2p, S 2p, Se 3d and Te 3d core level XPS measurements were carried out in a lab-based Thermo Scientific X-ray Photoelectron Spectrometer furnished with a monochromatic Al K_{α} photon source and a hemi-spherical analyser with total energy resolution close to 0.45 eV. The base pressure of the main chamber was below 2×10^{-8} mbar during XPS measurements. All three TiX_2 compounds were mechanically exfoliated just before XPS measurements to avoid any surface contamination. The bulk sensitivity of the measurements was increased by collecting the ejected photoelectrons in a surface normal geometry. Photon energy of the source was calibrated using C 1s core level spectra with a characteristic peak at around 284.6 eV binding energy. Each core level spectrum was decomposed in a casaXPS software using Gaussian-Lorentz type line profile.

XAS /XLD measurements: XAS/XLD measurements on three TiX_2 compounds were carried out at Ti $L_{3,2}$ edge at beamline 4.0.2 of the Advanced Light Source (ALS), at Lawrence Berkeley National Laboratory, USA. To avoid surface contamination, each single crystal was exfoliated mechanically in nitrogen atmosphere just before carrying out XAS measurements. No further surface treatments were performed as like vacuum heating or sputtering to clean the surface as these techniques could produce chalcogen vacancy in our systems. Total electron yield (TEY) detection technique were used during the XAS/XLD measurements.

Acknowledgement: J.C., Y.C. and B.P. are supported by the Gordon and Betty Moore Foundation EPiQS Initiative through Grant No. GBMF4534. X.L. and F.W. are supported by the U.S. Department of Energy (DOE) under Grant No. DOE DE-SC 00012375 for synchrotron work and bulk crystal characterization. This research used resources of the Advanced Light Source, which is a Department of Energy Office of Science User Facility under Contract No. DE-AC0205CH11231.

Keywords: Lattice distortion, dichalcogenides, XAS/XLD, electronic structure

* bp435@physics.rutgers.edu

† ywcao@nimte.ac.cn

¹ A. H. Castro Neto, F. Guinea, N. M. R. Peres, K. S. Novoselov,

A. K. Geim, *Rev. Mod. Phys.* **2009**, 81, 109.

² M. J. Allen, V. C. Tung, R. B. Kaner, *Chem. Rev.* **2010**, 110, 132.

³ S. Kumar, K. Chatterjee, *ACS Appl. Mater. Interfaces* **2016**, 8,

- 26431.
- ⁴ A.B. Frazier, R.O. Warrington, C. Friedrich, *IEEE Trans. Ind. Appl.* **1995**, 42, 423.
 - ⁵ C. Gong, H. Zhang, W. Wang, L. Colombo, R. M. Wallace, K. Cho, *Appl. Phys. Lett.* **2013**, 103, 053513.
 - ⁶ V. Podzorov, M. E. Gershenson, *Appl. Phys. Lett.* **2004**, 84, 3301.
 - ⁷ F. Xia, H. Wang, D. Xiao, M. Dubey, A. Ramasubramaniam, *Nat. Photonics* **2014**, 8, 899.
 - ⁸ K. F. Mak, J. Shan, *Nat. Photonics* **2016**, 10, 216.
 - ⁹ Q. H. Wang, K. K. Zadeh, A. Kis, J. N. Coleman, M. S. Strano, *Nat. Nanotechnol.* **2012**, 7, 699.
 - ¹⁰ B. W. H. Baugher, H. O. H. Churchill, Y. Yang, P. Jarillo-Herrero, *Nat. Nanotechnol.* **2014**, 9, 262.
 - ¹¹ M. Bernardi, M. Palummo, J. C. Grossman, *Nano Lett.* **2013**, 13, 3664.
 - ¹² L. Britnell, R. M. Ribeiro, A. Eckmann, R. Jalil, B. D. Belle, A. Mishchenko, Y. J. Kim, R. V. Gorbachev, T. Georgiou, S. V. Morozov, A. N. Grigorenko, A. K. Geim, C. Casiraghi, A. H. Castro Neto, K. S. Novoselov, *Science* **2013**, 340, 1311.
 - ¹³ S. Wi, H. Kim, M. Chen, H. Nam, L. J. Guo, E. Meyhofer, X. Liang, *ACS Nano* **2014**, 8, 5270.
 - ¹⁴ K. Tsutsumi, *Phys. Rev. B* **1982**, 26, 5756.
 - ¹⁵ A. M. Woolley, G. Wexler, *J. Phys. C* **1977**, 10, 2601.
 - ¹⁶ X. Xi, L. Zhao, Z. Wang, H. Berger, L. Forr, J. Shan, K. F. Mak, *Nat. Nanotechnol.* **2015**, 10, 765.
 - ¹⁷ P. Zhu, J. Cao, Y. Zhu, J. Geck, Y. Hidaka, S. Pjerov, T. Ritschel, H. Berger, Y. Shen, R. Tobey, J. P. Hill, X. J. Wang, *Appl. Phys. Lett.* **2013**, 103, 071914.
 - ¹⁸ J. Dai, E. Calleja, J. Alldredge, X. Zhu, L. Li, W. Lu, Y. Sun, T. Wolf, H. Berger, K. McElroy, *Phys. Rev. B* **2014**, 89, 165140.
 - ¹⁹ K. E. Ingle, K. R. Priolkar, A. Pal, R. A. Zargar, V. P. S. Awana, S. Emura, *Supercond. Sci. Technol.* **2015**, 28, 015015.
 - ²⁰ H.-X. Zhong, S. Gao, J.-J. Shi, L. Yang, *Phys. Rev. B* **2015**, 92, 115438.
 - ²¹ K. Deng, G. Wan, P. Deng, K. Zhang, S. Ding, E. Wang, M. Yan, H. Huang, H. Zhang, Z. Xu, J. Denlinger, A. Fedorov, H. Yang, W. Duan, H. Yao, Y. Wu, S. Fan, H. Zhang, X. Chen, S. Zhou, *Nat. Phys.* **2016**, 12, 1105.
 - ²² M. S. Whittingham, *Belgian Patent No.* 819672 **1973**;
 - ²³ Y. Gu, Y. Katsura, T. Yoshino, H. Takagi, K. Taniguchi, *Sci. Rep.* **2015**, 5, 12486.
 - ²⁴ X. Sun, P. Bonnick, L. F. Nazar, *ACS Energy Lett.* **2016**, 1, 297.
 - ²⁵ M. S. Whittingham, *US Patent No.* 4009052 **1976**.
 - ²⁶ R. R. Chianelli, J. C. Scanlon, A. H. Thompson, *Mater. Res. Bull.* **1975**, 10, 1379.
 - ²⁷ Y. Arnaud, M. Chevreton, *J. Solid State Chem.* **1981**, 39, 230.
 - ²⁸ J. Ishioka, Y. H. Liu, K. Shimatake, T. Kurosawa, K. Ichimura, Y. Toda, M. Oda, S. Tanda, *Phys. Rev. Lett.* **2010**, 105, 176401.
 - ²⁹ J.-P. Castellán, S. Rosenkranz, R. Osborn, Q. Li, K. E. Gray, X. Luo, U. Welp, G. Karapetrov, J. P. C. Ruff, J. van Wezel, *Phys. Rev. Lett.* **2013** 110, 196404.
 - ³⁰ H. Cercellier, C. Monney, F. Clerc, C. Battaglia, L. Despont, M. G. Garnier, H. Beck, P. Aebi, L. Patthey, H. Berger, and L. Forro, *Phys. Rev. Lett.* **2007** 99, 146403.
 - ³¹ J. A. Wilson, *physica status solidi (b)* **1978**, 86, 11.
 - ³² J. A. Wilson, *Solid State Commun.* **1977**, 22, 551.
 - ³³ H. P. Hughes, *J. Phys. C: Solid State Physics* **1977**, 10, L319.
 - ³⁴ K. Rossnagel, L. Kipp, M. Skibowski, *Phys. Rev. B* **2002**, 65, 235101.
 - ³⁵ R. Bianco, M. Calandra, F. Mauri, *Phys. Rev. B* **2015**, 92, 094107.
 - ³⁶ T. Rohwer, S. Hellmann, M. Wiesenmayer, C. Sohr, A. Stange, B. Slomski, A. Carr, Y. Liu, L. M. Avila, M. Kallne, S. Mathias, L. Kipp, K. Rossnagel, M. Bauer, *Nature* **2011**, 471, 490.
 - ³⁷ Z. Y. Wu, G. Ouvrard, P. Moreau, C. R. Natoli, *Phys. Rev. B* **1997**, 55, 9508.
 - ³⁸ C. Wan, X. Gu, F. Dang, T. Itoh, Y. Wang, H. Sasaki, M. Kondo, K. Koga, K. Yabuki, G. J. Snyder, R. Yang, K. Koumoto *Nat. Mater.* **2015**, 14, 622.
 - ³⁹ D. W. Bullett, *J. Phys. C* **1978**, 11, 22.
 - ⁴⁰ A. S. Shkvarin, Y. M. Yarmoshenko, N. A. Skorikov, M. V. Yablonskikh, A. I. Merentsov, E. G. Shkvarina and A. N. Titov, *Journal of Expt. and Theo. Phys.* **2012**, 114, 150.
 - ⁴¹ Y. Arnaud, M. Chevreton, *J. Solid State Chem.* **1981**, 39, 230.
 - ⁴² J. A. Wilson, A. D. Yoffe, *Adv. Phys.* **1969**, 18, 193.
 - ⁴³ E. Stavitski, F. M. F. de Groot, *Micron* **2010**, 41, 687.
 - ⁴⁴ D. I. Khomskii, *Transition Metal Compounds*, Cambridge University Press
 - ⁴⁵ A. Simunek, O. Sipr, S. Bocharov, D. Heumann, G. Drager. *Phys. Rev. B* **1997**, 56, 19.